The Journal of Experimental Biology 209, 43-56
Published by The Company of Biologists 2006
doi:10.1242/jeb.01958

Induced airflow in flying insects

II. Measurement of induced flow

Sanjay P. Sane* and Nathaniel P. Jacobson
Department of Biology, University of Washington, Seattle, WA 98195, USA
*Author for correspondence (e-mail: sane@u.washington.edu)

Accepted 21 October 2005

Summary

The flapping wings of insects and birds induce a strong flow over their body during flight. Although this flow influences the sensory biology and physiology of a flying animal, there are very little data on the characteristics of this self-generated flow field or its biological consequences. A model proposed in the companion paper estimated the induced flow over flying insects. In this study, we used a pair of hot wire anemometers to measure this flow at two locations near the body of a tethered flapping hawk moth, *Manduca sexta*. The axial inflow anemometer measured the airflow prior to its entry into the stroke plane, whereas the radial outflow anemometer measured the airflow after it crossed the stroke plane. The high temporal resolution of the hot wire anemometers allowed us to measure not only the mean induced flow but also subtle higher frequency disturbances occurring at 1–4 times the wing beat frequency. These data provide evidence for the predictions of a mathematical model proposed in the companion paper. Specifically, the absolute value of the measured induced flow matches the estimate of the model. Also, as predicted by the model, the induced flow varies linearly with wing beat frequency. Our experiments also show that wing flexion contributes significantly to the observed higher frequency disturbances. Thus, the hot wire anemometry technique provides a useful means to quantify the aerodynamic signature of wing flexion. The phasic and tonic components of induced flow influence several physiological processes such as convective heat loss and gas exchange in endothermic insects, as well as alter the nature of mechanosensory and olfactory stimuli to the sensory organs of a flying insect.

Key words: hot wire anemometry, *Manduca sexta*, wing flutter, odor tracking, convective heat loss, airflow sensing.

Introduction

Like rotating propeller blades, flapping wings of an insect draw air from above the wing and generate flight forces by imparting momentum to this air. Thus, a natural consequence of any flapping activity is an induced airflow along the body of the insect. This flow envelops the flying insect and influences many flight-related physiological and sensory processes. Airflow sensors (Gewecke, 1970; Horsmann et al., 1983), olfactory sensors (Loudon and Koehl, 2000), heat exchange (Heinrich, 1993; Roberts and Harrison, 1998) and various mass exchange processes such as oxygen, carbon dioxide and water (Wasserthal, 2001), are all profoundly affected by the structure of such flows. Thus, there exists a biophysical feedback relationship between the wing kinematics and flight-related sensory-motor physiology that is entirely mediated by the external air medium.

One important biological consequence of induced airflow is its influence on mechanosensory and chemosensory organs, which receive their stimulus *via* the surrounding fluid medium. For example, the flightless silkworm moth *Bombyx mori* actively fans its wings to increase the air flux over its body, thereby enhancing the rate at which its antennae encounter odor molecules (Loudon and Koehl, 2000). In flying locusts, wind sensory hairs located on the head are activated by motion of the head and induced air flow and provide phasic input entraining the flight motor output (Horsmann et al., 1983). These few examples illustrate how flying animals rely on the mechanical feedback from their surrounding fluid medium to perceive mechanosensory and chemosensory cues. However, in many important areas of research, the role of the feedback mediated *via* induced airflow remains under-appreciated. For example, we know very little about how entrainment of the upwind fluid due to flapping activity affects odor sampling and odor tracking during flight (Willis and Arbas, 1991; Vickers, 2000). In addition to the sensory biology, induced airflow also influences the thermal biology of flying insects through enhanced convection. Yet, although there are several detailed studies and related models on thermoregulation in flying insects that emphasize convection as a dominant mode of heat loss, none account for the enhancement in convective heat loss from induced airflow

(Church, 1959; for reviews, see Heinrich, 1993; Roberts and Harrison, 1998).

To some extent, induced airflow in actively flapping insects may have been overlooked due to the lack of data on flow fields around a flying insect. There are several available methods for measurement of flows around flapping insect wings (for a review, see Sane, 2003). In larger insects and birds, it is increasingly possible to image these flows with fine spatial resolution using modern techniques such as smoke visualization combined with high-speed videography (hawk moths, Ellington et al., 1996; Willmott et al., 1997; butterflies, Brodsky, 1991; Grodnitsky and Morozov, 1992; Srygley and Thomas, 2002) and digital particle image velocimetry (DPIV; flies, Dickinson and Gotz, 1996; hawk moths, Bomphrey et al., 2005; hummingbirds, Warrick et al., 2005). While DPIV offers a fine spatial quantification of flow fields with resolutions previously not possible, it remains limited in its ability to acquire and store the data at the frequencies typical of insect wing beats. Hence, DPIV studies on actual animals have typically not been able to explore the finer temporal aspects of flow. Similarly, smoke visualization techniques are able to capture flows with a good spatial and temporal resolution but do not offer an easy means to quantify these flows. In contrast, traditional flow measurement techniques such as hot wire anemometry, although poor at determining the spatial variation in the flow field, offer an excellent temporal resolution of the flows around the bodies of flying insects (bats, Norberg et al., 1993, insects, Bennett, 1970; Loudon and Koehl, 2000) and in their wakes (Lehmann, 1994). Using hot wire anemometry, it is possible to address how flapping wings affect the temporal dynamics of flows due to flapping and, furthermore, how such time-variation affects delivery of the airborne stimuli to the sensory organs of insects.

To understand how flight activity and related flow disturbances influence the fluid-mediated mechanical feedback in flying insects, it is first necessary to estimate and measure induced airflow. In a companion paper, we outlined a theoretical framework to calculate the mean induced flow in a flying insect (Sane, 2006). Here, we measure induced airflow on tethered hawk moths *Manduca sexta*, with high temporal sensitivity. These insects are convenient to work with because they flap readily and uninterruptedly under tethered conditions. They also present an interesting experimental system in which all of the physiological effects of induced airflow outlined above are likely to be important. Not surprisingly, they are also one of the best-studied organisms for thermoregulation (Heinrich, 1971; for a review, see Heinrich, 1993). Using hot wire anemometry, the airflow was measured at two point locations: an axial inflow location between the antenna and a radial outflow location above the thorax. This paper also showcases the power of conventional hot wire anemometery as a remarkable tool to study aerodynamics of flying insects due to its high temporal sensitivity. These studies reveal that in addition to the gross flow predicted by the theory, the flows contain higher frequency fluctuations that may be of considerable biological importance.

Materials and methods

Hot wire anemometry

In all experiments, the magnitude of airflow was measured using Kurz 490M constant temperature mini-anemometers (Kurz Instruments, Inc., Monterey, CA, USA). The standard version of this anemometer has a galvanometer-readout. The maximum measurement error of the anemometer, as described by the specifications manual, is $5\pm0.005\%/^{\circ}C + 0.1$ m s^{-1}. This least count is rather large for airflow measurements generated by a flapping moth (typically ranging from 0.2–4.0 m s^{-1}; see Results). Moreover, because the inertia of the moving needle is substantial, the calibrated galvanometer cannot reliably capture the rapid changes in air speed magnitude. In contrast to the galvanometer needle movement, the actual voltage measurements tapped from the anemometer are far more sensitive to small or rapid changes in air speed around a flapping insect. The least count for this voltage readout was determined to be $5\pm0.005\%/^{\circ}C$ in addition to a negligible digitization error. The anemometer filament itself is insensitive to the direction of the flow, but is encased in a cylindrical shield that allows predominantly unidirectional flow, thus enabling rectified readings of the airflow.

Wind tunnel construction

The calibration of the airflow was carried out within a custom Plexiglas wind tunnel. The area of the square working section of the wind tunnel was 15 cm×15 cm. The laminarity of the flow within the working section of the wind tunnel was established using a pre-calibrated anemometer (Kestrel 3000, Richard Paul Russell Ltd, Lymington, UK) in combination with smoke visualization. For a given position within the wind tunnel, a constant reading of the anemometer indicated that there were no temporal changes in the flow pattern at that point. Similarly, a constant reading of the anemometer between any two or more arbitrary points within the working area indicated that there were no significant spatial gradients of velocity within the working area of the wind tunnel. Thus, for a given setting of the motor speed of the wind tunnel exhaust fan, it was always possible to assign a single value for the air speed.

Anemometer calibration

To establish the precision and accuracy of anemometric readings, we calibrated the anemometer readout in a custom wind tunnel using two separate methods. In one method, to ensure initially that the anemometer galvanometer was reliable, we adjusted the wind tunnel motor speed to a fixed value and confirmed that these readings held steady for a given motor speed. We then changed the wind tunnel motor speed to random high or low values using a controller. After the initial transients, we read the steady needle reading in each of the two anemometers. Because readings from both anemometers always matched over a wide range of speeds of the wind tunnel and they always showed the same values for any given wind tunnel controller settings, we concluded that the anemometers read-outs are reasonably precise, i.e. they are repeatable. In a second method, we determined the accuracy of the two

anemometers by comparing their values with those of a standard propeller anemometer (Kestrel 3000) placed within the working section. The values of air speed measured by both types of anemometers matched to about 0.05 m s^{-1}, indicating that their values are reasonably accurate in the range tested (0–4 m s^{-1}). Using these measurements, the anemometers were calibrated to obtain air speeds from voltage measurements. All anemometry described in these papers was carried out using the analog voltage readout.

Anemometer frequency response

To assess the frequency response of the anemometer, we connected a dual-mode mechanical lever system (Aurora Scientific Inc., Aurora, ON, Canada) to an approximately 33 mm×21 mm rectangular control wing made of balsa wood (Fig. 1A). When oscillated at various frequencies, this artificial wing generated periodic disturbances in air which were recorded by an anemometer placed very close (approx. 1 cm) to the artificial wing. Using this apparatus, the anemometer's frequency response was tested at 10, 50, 100, 200 and 300 Hz with variable amplitudes (<1 cm), respectively, while simultaneously recording the frequency of the servomotor. Although some lateral movement of the control wing introduces some lower frequency contributions to the recorded anemometric signal, there was always a sharp and distinct airflow signal at exactly the frequency of artificial wing oscillation (Fig. 1B). The maximum anemometric recording using this apparatus was 300 Hz, more than 10 times the wing beat frequency of the hawk moths under study. Beyond this frequency, the mechanical integrity of our apparatus broke down and it was not possible to determine the maximum limit of the anemometer's frequency response.

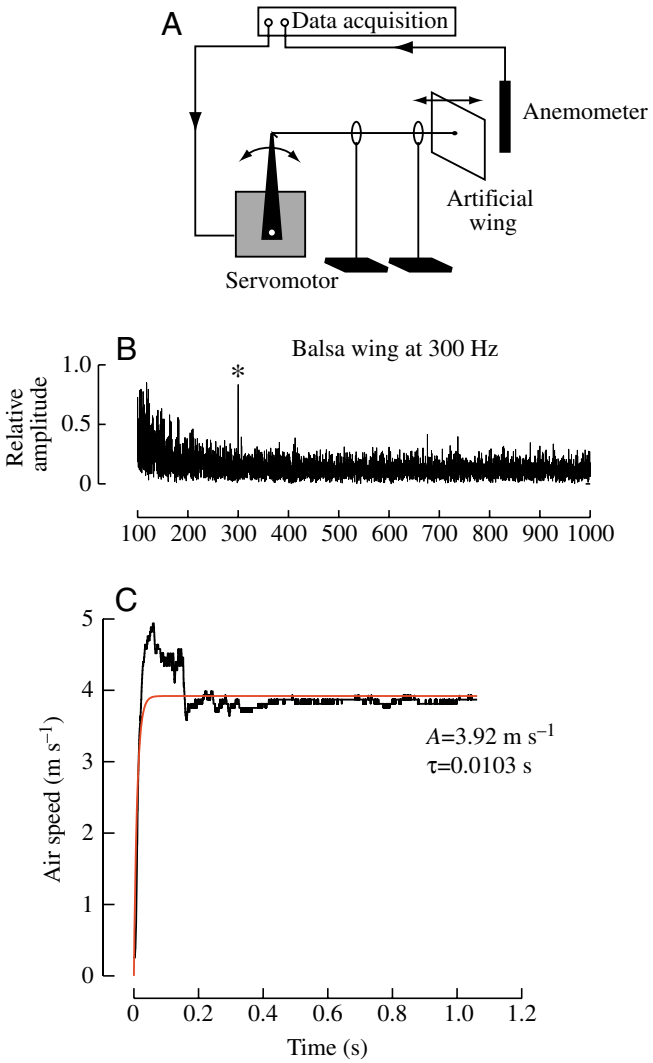

Fig. 1. Anemometer calibration. (A) A servo motor driven at up to 300 Hz drives a balsa wood plate. The air disturbance generated as a result of this oscillation is clearly registered as a pulse in the anemometric record (B). Thus, the anemometer has a frequency response of at least 300 Hz. (C) The time taken by the anemometer to reach its steady value has a time constant τ of 0.0103 s, nearly 1/4 of the wing period (ca. 0.04 ms). *A*=airspeed; the red line indicates the exponential function $A_0(1–e^{t/\tau})$; see text for details.

Anemometer time constant

To determine how rapidly the anemometer reading reaches its steady value, we characterized the time constant τ for an anemometer using a step input of air speed from zero to a constant value. The airflow in the wind tunnel was initially held at a constant speed of 3.92 m s^{-1}. We then placed the anemometer inside a small but deep hole in the wall with no airflow. After the needle was steady at the zero value for a few seconds, we plunged the anemometer rapidly into the wind tunnel. Following an initial peak due to the disturbances associated with the motion of the anemometer in moving air, the anemometer readings rapidly stabilized to a steady value of 3.92 m s^{-1}. We fitted the measured airspeed with an exponential function $A_0(1–e^{t/\tau})$, where A_0 is the asymptotic average speed of the airflow and τ is the time constant of the anemometer. Due to limitations on how fast the anemometer can be manually plunged and the time it takes for the resultant fluid disturbance to dissipate, the value of this time constant only provides a conservative estimate of the actual time constant of the anemometer. For the Kurz 490 anemometer used in these experiments, we measured a time constant of 0.0103 s (Fig. 1C), corresponding to a frequency of 97 Hz. This is nearly four times the wing beat frequency of a typical *Manduca sexta* wing. Although the anemometer can register frequencies higher than 97 Hz, these time constant values suggest that they do not provide a reliable value for the airspeed of events occurring at frequencies above 97 Hz.

Measurement of induced airflow

The adult moths *Manduca sexta* (Linnaeus) used in these experiments were collected from the colony maintained in the Department of Biology at the University of Washington. The moths were kept at a temperature of 26°C with a 17 h:7 h L:D photoperiod, and were used within a week of eclosion. The data presented here was collected from 12 moths. Each moth

was cold-anesthesized in a freezer for approximately 12 min. After freezing, we weighed the moth and placed it upside down in a 'V' shaped metal trough. The scales surrounding the meta-thoracic episternum were removed by a low pressure air source, and the cuticle of the meta-thoracic episternum was scratched a few times with a scalpel blade to create a better gluing surface.

A tether post was made from a 6 mm×6 mm×0.25 mm rounded brass plate soldered to the end of a brass rod that was 50 mm in length and had a diameter of 2 mm. The overlap between the plate and the rod was 2 mm. The end of the tether plate was attached to the metathoracic episternum on the underside of the moth using cyanoacrylate glue and baking soda. The tether post was positioned at a 40° angle with respect to the moth's body. The glue was allowed to set for 10 min with the moth immobilized. During the setting time, we measured the length of the wings, body and antennae. The tether post was secured to a 99 mm×19 mm×2.5 mm horizontal aluminum beam forming a force sensor. The vertical deflections of the beam and tether post are linearly proportional to the vertical forces exerted by the moth for small deflection angles (such that $\sin\theta \sim \theta$ when $\theta \sim 0$). Vertical deflection of the beam was measured by mounting a first-surface mirror on the end of the beam and reflecting a laser from the mirror onto a vertical optical sensor strip. The output of the sensor strip was converted by an analog divider circuit to produce a voltage signal, which varies linearly with the vertical force exerted on the beam (Fig. 2A).

We placed a pair of hot wire anemometers (Kurz 490M mini-anemometers modified to get the analog voltage readout as described in the section on anemometry) at fixed near-field positions along the midline of tethered, actively flapping hawk moths. One anemometer (or the 'axial inflow anemometer') was placed at roughly the mid-point between the antennae. A second anemometer (or the 'radial outflow anemometer') was placed at a radial position at roughly 3/4 of the wing length from the base (Fig. 2A). The anemometric data acquired at these positions allowed us to determine the changes of induced airflow and test predictions of a theoretical model proposed in the companion paper (Sane, 2006).

To induce flapping, the tethered moths were presented with a continually varying visual stimulus on the LCD monitor placed in front of it (Fig. 2A). Tethering the insect allowed us to accurately maintain a steady distance between the insect and the anemometers. Although the LCD monitor was used to motivate the insects to fly, in all the experiments reported here we turned off the visual stimulus after the moth initiated flapping to limit visual influence on wing kinematics. We allowed the insect to flap for at least 10 s after the LCD monitor had been turned off and then closed the lid of the flight chamber to reduce ambient light. Although this does not ensure that insects will flap with steady kinematics, it does assure us that the visual stimulus did not contribute significantly to changes in wing flapping frequency or amplitude.

Because the time constant of the anemometers is about 1/4 of the stroke period, it was possible to measure induced flow

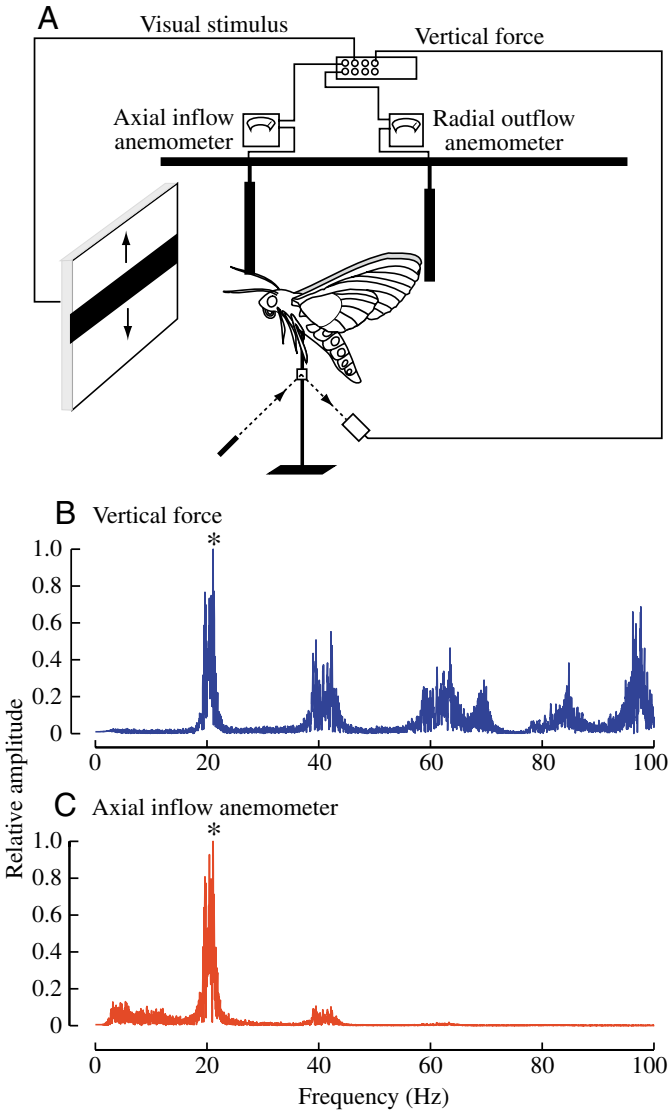

Fig. 2. Measurement of induced air flow in a flight chamber. (A) Two anemometers, an axial inflow anemometer and a radial outflow anemometer, placed between the antennae and behind the wings at roughly 3/4 of the wing length from the base, respectively, recorded the induced airflow due to the flapping wings. An optical force sensor simultaneously recorded the vibrations generated by the flapping moth on its tether. A computer-controlled visual display motivated the moth to fly and modulate its wing kinematics. In the experiments reported here the visual display was turned off after the moth initiated flight and the chamber was left dark. (B,C) The frequency peaks of the vertical measurements and the two anemometric records (only axial inflow data are shown) always matched the primary stroke frequency (asterisks) and a secondary peak at double stroke frequency.

at the time scales of flapping wings. We verified that the periodicity of the flow measured by both anemometers matched the periodicity of the corresponding record from the vertical force beam recording the wing vibrations (Fig. 2B), thus ascertaining that the anemometers accurately measured the aerodynamic result of wing movement. The force beam record itself cannot accurately measure aerodynamic force

because it integrates the aerodynamic and inertial input from the two pairs of wings and the body in addition to the resonant properties of the force beam itself (resonance in horizontal direction was 71 Hz and in vertical direction was 96 Hz). However, the vertical force record was highly sensitive to wing motion and thus could be used to independently determine stroke frequency. Whereas the anemometric record showed clear peaks at the driving or wing beat frequency (for example, ca. 20 Hz in Fig. 2C) and much diminished peaks at higher frequencies, the force beam record shows several large peaks at multiple harmonics of the fundamental frequency (Fig. 2B,C). Because the anemometers and force beam are mechanically uncoupled, a perfect matching of the dominant period from these two records indicated that the anemometer readings precisely captured the periodic airflow fluctuations due to the beating wings at both the upstream and downstream locations.

All voltage data from the actual moths were acquired using a National Instruments Data Acquisition card (Austin, TX, USA; PCI-MIO 16E-4) attached to a Multiple Input-Output (MIO) BNC-2090 adapter (National Instruments) at 4000 Hz. Data from the artificial wing experiments was acquired on the same system at 10 000 Hz. A custom graphic user interface was programmed in MATLAB (The Mathworks, Inc., Natick, MA, USA) to simultaneously acquire the data and send output commands.

Spectral analysis of anemometric measurements

The high sensitivity of the anemometric measurements allowed us to perform a detailed analysis on these data to determine their spectral properties. The data for all bouts of all moths were Fourier transformed using custom MATLAB programs and plotted as a function of frequency *vs* amplitude of the underlying periodic phenomena. When discussing them individually, these moths will be referred to as Moth 1 through 12, for convenience.

A first analysis involved a standard Fourier transformation of the entire raw time series. Because the lengths of these records vary from trial to trial, the frequency resolution (inverse of the total time length of the record) varies from one trial to another.

These analyses allowed us to determine the frequency composition of the records and identify the principal frequency components of each time series. To selectively focus on the higher frequency contributions due to flapping wings, when presenting these data in Fig. 4, we eliminated these low frequency contributions by operating a high-pass, 4-pole Butterworth filter on the data with a cutoff at 3 Hz.

In a second method, because a standard Fourier transform may sometimes de-emphasize the relatively smaller frequency peaks in a distribution, we estimated the power spectrum using the Welch's Overlapped Segment Averaging (WOSA) method (Percival and Walden, 1993). This method allowed us to reduce the variance of the spectral estimate, with the trade-off that spectral resolution also decreased. In this method, the time series was first divided into multiple overlapping time blocks. For each block, we subtracted the signal mean and multiplied by a Hann taper to reduce transient effects, followed by a Fourier transform on each tapered block. The squared magnitude of each transformed block was then averaged together to form the WOSA estimate. In the experiments described here, we used a block size of 128 000 samples (32 s) with 50% overlap between blocks, which gives a frequency resolution of 0.0606 Hz. This resolution is more than 400 times finer than the typical wing beat frequency of 25 Hz.

The results of these analyses are plotted in Fig. 4 for the sample cases of Moth 7 and Moth 12. The standard Fourier transforms for axial inflow records are shown in Fig. 4A (Moth 7) and Fig. 4C (Moth 12) and for the radial outflow records are shown in Fig. 4E (Moth 7) and Fig. 4G (Moth 12). The corresponding WOSA plots are in Fig. 4B,D,F,H respectively. A summary of the Fourier data for all moths is provided in Table 1.

In a third analysis, we determined the effect of wing beat frequency on mean air flow. For this analysis, we focused on 5 of the 12 moths, which (i) flew uninterruptedly for at least 150 s at a wing beat frequency representative of normal flight (20–30 Hz), and (ii) showed greater variation in wing beat frequency. For these records, the air speed time-series was subdivided arbitrarily into 1 s time bins for further analysis because a 1 s time bin was able to include most wing beats within that time bin while still capturing the functional relationship between the mean air flow and stroke frequency. Thus, in the subsequent analysis, we assumed that every second of flight was independent of the following or preceding seconds. Although not strictly valid for wing beats in an immediate sequence, this assumption is reasonable for majority of the wing beats within two sequential time bins. Each second of flight thus obtained was Fourier transformed to measure the instantaneous wing beat frequency and the mean airspeed. Because the Fourier analysis is carried over 1 s at a time, the minimum frequency resolution of these data was 1 Hz. A summary of these data are provided in Fig. 5 and Table 2 for all 5 moths chosen for the study.

Experimental investigation of higher frequency peaks

To determine the consequences of wing flexion on the aerodynamic signature of flapping wings, we used the apparatus illustrated in Fig. 1A and described in the section on anemometer calibration. This apparatus allowed us to rapidly oscillate an artificial wing back and forth and measure the resulting anemometric signal at preset frequencies. We generated periodic air disturbances using to two types of artificial wings by oscillating them back and forth at 50 Hz. The first wing, made of balsa wood, was rigid and did not flex at these frequencies. The second wing, made of paper, was flexible and fluttered considerably when oscillated back and forth at 50 Hz. An anemometer placed very close to the oscillating airfoil and aligned near the center of the rectangular wing measured the periodic air disturbances due to the oscillating plate. This ensured that the periodic edge-related

Table 1. *Summary of Fourier analysis of the longest flight bouts of each moth*

		First peak (Mean air speed = Amplitude/2)			Second peak (wing beat frequency)		Third peak	
Moth	Longest flight bout (s)	Frequency (Hz)	Amplitude ($m\ s^{-1}$)	Mean air speed ($m\ s^{-1}$)	Frequency (Hz)	Amplitude ($\times10^{-3}\ m\ s^{-1}$)	Frequency (Hz)	Amplitude ($\times10^{-5}\ m\ s^{-1}$)
Axial inflow								
1	224.3	0	0.192	0.096	15.81	1	31.7	8.1
2	53.3	0	0.375	0.188	21.07	7.3	42.2	74.8
3	73.2	0	0.287	0.144	20.93	6.4	42.98	13.9
4	28.7	0	0.261	0.131	24.56	6.8	49.09	79.3
5	234.7	0	0.364	0.182	27.76	2.5	52.02	27.2
6*	234.2	0	0.447	0.224	26.5	4.6	53.0	41.5
7*	178.1	0	0.534	0.267	23.73	12.9	46.98	167.6
8	16.4	0	0.346	0.173	17.62	14.8	35.24	141.6
9*	135.9	0	0.365	0.183	20.26	7.0	41.01	42.8
10	12.7	0	0.202	0.101	17.09	6.8	35.59	96.8
11*	278.2	0	0.361	0.181	20.42	4.3	40.9	39.9
12*	323	0	0.395	0.198	20.84	5.2	41.53	35.79
Radial outflow								
1	224.3	0	0.4767	0.238	15.69	7.1	30.9	193.9
2	53.3	0	0.8413	0.421	20.75	20.3	42.2	933.4
3	73.2	0	0.2498	0.125	20.18	3.9	–	–
4	28.7	0	0.679	0.34	24.6	22.2	49.1	211.3
5	234.7	0	0.6384	0.319	–	–	–	–
6*	234.2	0	1.03	0.52	26.67	14.83	52.16	331.1
7*	178.1	0	3.22	1.61	23.73	95.23	46.47	2606
8	16.4	0	1.43	0.72	17.44	80.72	34.57	2783
9*	135.9	0	1.43	0.72	20.06	40.16	40.17	1264
10	12.7	0	0.65	0.33	17.64	27.84	–	–
11*	278.2	0	2.96	1.48	20.42	91.8	39.83	1911
12*	323	0	3.82	1.91	20.84	37.3	41.64	814.8

*Animals used for regression analysis because they offered a long time record and a sufficient frequency spread.

disturbances to the airflow were minimal and most of the airflow measured by the anemometer was along a single axis due to the relatively simple back and forth motion of the volume of air close to the rectangular plate.

Results

Self generated airflow in hawk moths

The continuous airflow records of the axial and radial anemometers at three time scales of the order of 10^2, 10^1 and 10^0 s are shown for a sample flight bout in Fig. 3A–C and D–F, respectively. A flight bout is defined here as any continuous, uninterrupted flight record lasting for more than 10 s (or at least 200 wing beats).

Moreover, in all cases the flight bouts were recorded after the moths had already been flapping for a few minutes, thus allowing them to warm up sufficiently. Although this procedure minimizes the possibility of capturing the 'warming-up' mode of flapping, we cannot fully rule out the possibility that some of the flapping was associated with thermogenesis in absence of simultaneous measurements of the thoracic temperatures.

At the scale of 10^2 s, the airflow shows a wide range of values depending on the changes in kinematics of the flapping wings. The magnitude of axial inflow is much lower than the radial outflow. For instance, in the sample flight bout shown in Fig. 3A–C the axial inflow measured between the antennae ranges between 0 and 0.52 $m\ s^{-1}$ as compared to the radial outflow range of 0 to 3.55 $m\ s^{-1}$ for the identical flight bout in Fig. 3D–F. At the scale of 10^1 s, the measurements at these two locations show a greater fluctuation in the radial outflow than axial inflow (Fig. 3B,E). At the scale of 10^0 s at both locations, the measurements reveal a clear periodicity in the airflow records due to oscillatory wing motion (Fig. 3C,F). The 24 peaks seen in the 1 s upstream record in Fig. 3C each represent a wing beat of the flapping moth. Because the period of each wing beat (ca. 0.04 s) is approximately four times the time constant of the anemometers (ca. 0.01 s), the peak amplitudes capture the full range of the actual signal. The periodicity of axial inflow is considerably more regular than the radial outflow, indicating that the radial outflow anemometer captures much of the unsteadiness due to the complex aerodynamic perturbations caused by wing rotations and wing-wing interactions at dorsal stroke reversal. Fig. 3C shows a range of axial inflow from

0.19–0.36 m s^{-1} whereas the range of radial outflow in Fig. 3F is slightly higher and between the values of 0.8–2.8 m s^{-1}.

Spectral properties of the anemometric records

In all the experiments reported here, we turned off the LCD monitor and closed the flight chamber lid to remove the visual stimuli to the tethered moths. Thus, any changes in wing kinematics may be interpreted as 'voluntary'. The Fourier transforms of the time series data (Fig. 4A,C,E,G) of the airflow generated by these kinematics typically showed a fixed pattern of peaks occurring at (i) wing beat frequency, (ii) twice the wing beat frequency, and in a few cases (iii) three times the wing beat frequency, in addition to the initial offset at 0 Hz, representing the mean induced air flow about which the higher frequency fluctuations occur. However, in many cases, several higher frequency peaks not obvious in the standard Fourier plots are revealed by the WOSA plots (Fig. 4B,D,F,H), suggesting that this type of time-series analysis may be particularly useful in analysis of hot wire anemometric data of high frequency flapping. This section focuses primarily on the first three peaks observable in every bout of every moth tested.

To highlight the effect of second and third peaks due to wing beat frequency and its double, the data presented in Fig. 4 were filtered under 3 Hz to eliminate the offset value and other lower frequency components that typically overwhelm other higher frequency contributions in long time series records. Also in Fig. 4, the Fourier plots are normalized with respect to the maximum peak to allow easy comparison of the relative contributions of the higher frequency contribution with respect to the dominant wing beat frequency component.

Fig. 4A,C,E,G shows two samples (Moth 7 and Moth 12) of the Fourier records from the 12 moths in this study. Fig. 4A,C shows the Fourier transforms of axial inflow anemometric data for the longest flight bouts in these two sample cases and Fig. 4E,G shows similar data for the radial outflow anemometer. Moth 7 (Fig. 4A,B,E,F) flew for about 178 s and Moth 12 (Fig. 4C,D,G,H) flew for 323 s. Because the frequency resolution of the Fourier transformed data is the inverse of the length of the time record, the Fourier transformed data have different resolutions. Specifically, shorter time records have a coarser frequency resolution whereas the longer time records have a comparatively finer resolution of

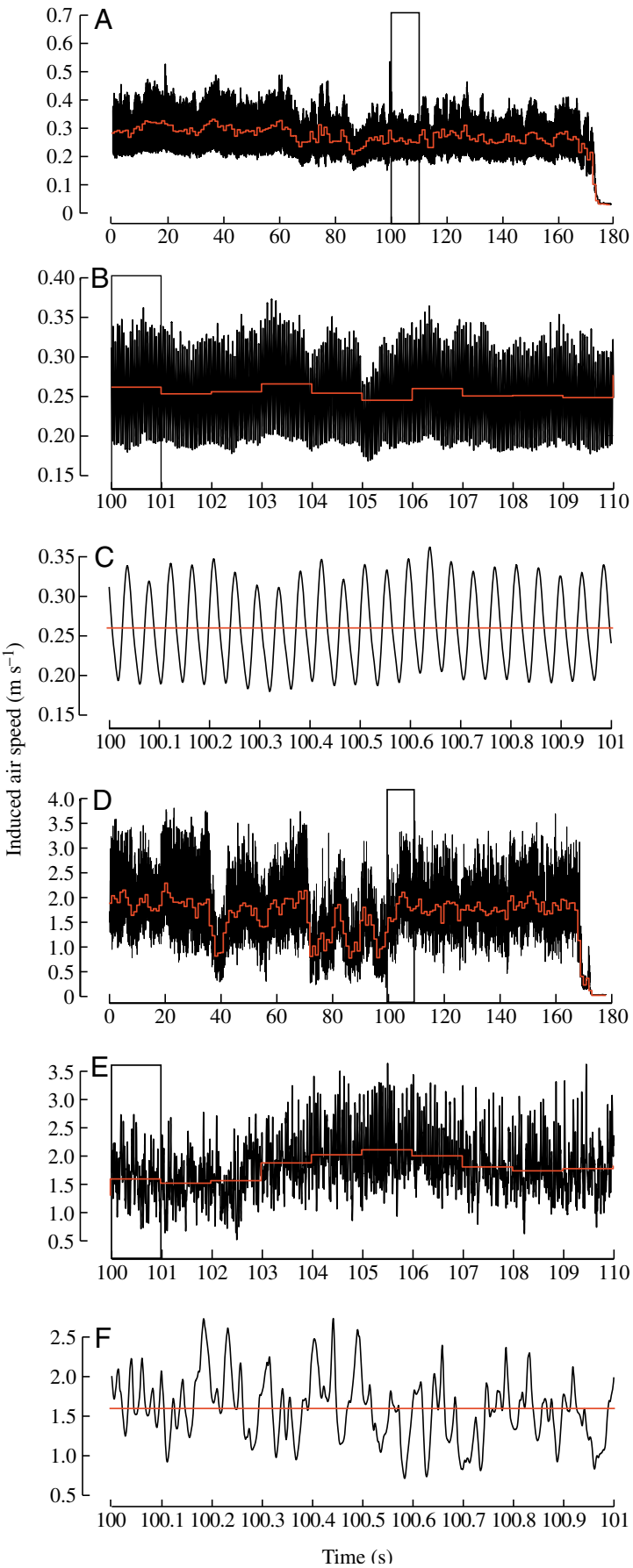

Fig. 3. Raw anemometric data. (A–C) Axial inflow. The data are shown here at time scales of (A) 10^2 s, (B) 10^1 s and (C) 10^0 s for axial inflow in a sample flight bout for Moth 7. (D–F) Radial outflow. The data are shown here at time scales of (D) 10^2 s, (E) 10^1 s and (F) 10^0 s. In these graphs, the red lines are averages over each second of recording. B and E are expanded records of the insets in A and D, respectively, and C and F are expanded records of the insets in B and E, respectively.

frequency. However, even the lowest resolution in the Fourier data was 0.08 Hz (for Moth 10), which is more than two orders of magnitude lower than the wing beat frequency. The absolute amplitude of the transform at each frequency presented in Table 1 thus represents the average amplitude of airspeed fluctuation at that frequency.

The data from Moths 7 and 12 showcase some of the key general features of the induced airflow discussed in this section. First, there is always a peak at wing beat frequency; however, this peak may be sharp or diffuse, depending on the degree to which the moth varied its stroke frequency within each flight bout. For example, Moth 7 in Fig. 4A,B,E,F shows a rather steep peak at wing stroke frequency with very little spread around this peak, suggesting that it maintained its wing beat frequency in a very narrow range. In contrast, Moth 12 in Fig. 4C,D,G,H shows a substantial spread of wing stroke frequency with more than one peak, suggesting that it varied its stroke frequency within the flight bout. Second, the airflow signal contains information about the subtler phasic phenomena occurring at frequencies higher than stroke frequency. This is particularly evident in the WOSA plots (Fig. 4B,D,F,H). All the plots shown in Fig. 4 (and summarized in Table 1) show a prominent peak at precisely double the wing beat frequency in addition to the peak at wing beat frequency. If the wing beat frequency peak is sharp, then the higher frequency peaks are also sharp (Fig. 4A,B,E,F for example). On the other hand, if the moth varies its stroke frequency to cause a spread in the stroke frequency peak, then a similar spread is evident in the higher frequency peaks (Fig. 4C,D,G,H for example). This suggests that the higher frequency events are closely tied to the aerodynamic events within each wing stroke. Further, the ratio between the magnitude of the first and second peaks tends to be greater in the inflow recordings as compared to the outflow recordings (Fig. 4A,E,C,G). This suggests that the higher frequency disturbances are relatively more attenuated upstream of the wings (against the mean air flow) than downstream (along the mean airflow). Further, as revealed by the WOSA plots, more high frequency peaks are visible in the axial inflow record as compared to the radial outflow record, suggesting that, in general, the signal-to-noise ratio is better at the axial inflow location than at the radial outflow location.

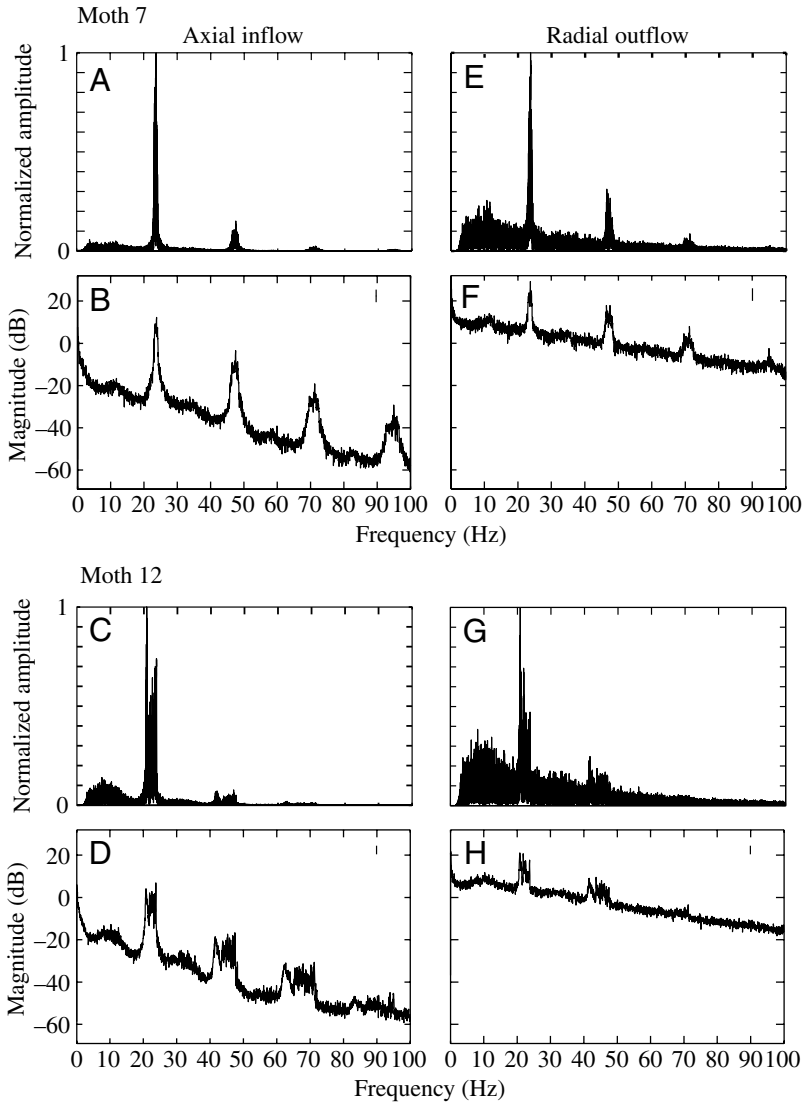

Fig. 4. Spectral characteristics of the induced flow. (A–D) Axial inflow and (E–H) radial outflow spectral data for the sample case of Moth 7 (A,B,E,F) and Moth 12 (C,D,G,H). For each moth, the top panels show standard Fourier plots (Moth 7: A,E; Moth 12: C,G) and lower panels show the Welch's Overlapped Segment Averaging (WOSA) plots (Moth 7: B,F; Moth 12: D,H). A vertical bar in each of the WOSA plots shows the 95% confidence interval for the spectral estimate.

Because anemometers are mechanically decoupled from the rest of the apparatus and from each other, the co-occurrence of the various peaks in the two anemometers and the force beam data suggests that these higher frequency peaks are not artefacts. Rather, these peaks reveal the air disturbances caused by aerodynamic events occurring at least twice at every wing beat. Finally, the frequency contributions below 10 Hz arise from the slower and more persistent changes in the flow velocity lasting over several wing strokes. Table 1 also reveals the variability in the range of frequencies of each moth as well as the differences between moths. Typical sustained flapping frequencies of moths tested in these experiments ranged from 14 Hz to 28 Hz, excluding rare (<1 s) bouts of 30 Hz or more. Presently, it is not clear to what extent these differences are due to tethering, nor can we fully rule out the possibility that some of the lower frequency bouts may be associated with thermogenesis rather than flight. For example, the dominant frequency peak for Moth 1 is around 16 Hz (Table 1) with minor fluctuations about this value. Although this moth had been flapping for

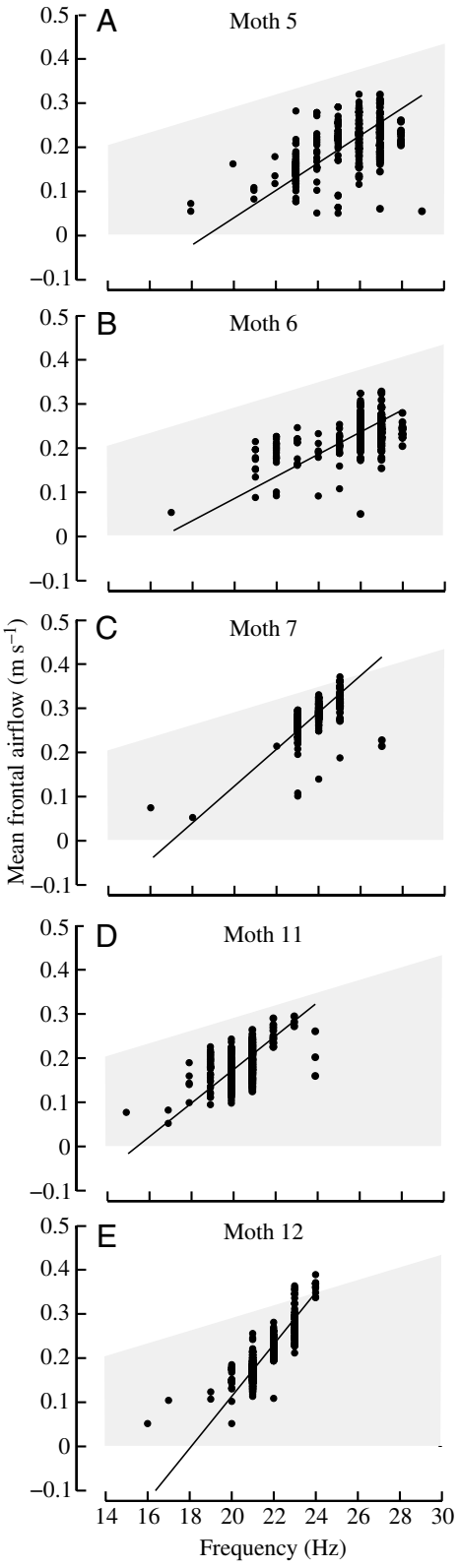

Fig. 5. Mean axial flow as a function of wing beat frequency. The anemometric time series from all bouts from Moth 5 (A), Moth 6 (B), Moth 7 (C), Moth 11 and Moth 12 (B) were divided into 1 s bins and the peak wing beat frequency for each bin was plotted against the mean value of the airflow over that bin. The grey area in the background describes the range of values predicted by Eqn 1.

Table 2. *Mean axial inflow vs wing beat frequency in flapping moths*

Moth	Slope	*y*-intercept	Record length (s)	r^2
5	0.03	–0.60	294	0.32
6	0.03	–0.42	331	0.28
7	0.04	–0.71	229	0.42
11	0.04	–0.59	360	0.24
12	0.06	–1.06	472	0.72

more than 5 min, we cannot completely rule out the possibility that it was still undergoing thermogenesis.

Dependence of induced airflow on wing beat frequency

How does an increase in wing beat frequency influence the induced airflow? To address this question, we investigated five moths which flapped continuously for over 150 s and showed some variability in their wing beat frequency. Fig. 5 shows plots of mean airspeed as a function of wing beat frequency for these five moths labeled Moths 5, 6, 7, 11 and 12. A summary of the regression data is given in Table 2. Because these records were chopped into 1 s bins for analysis, the Fourier analysis of each second of flight offers a maximum frequency resolution of 1 Hz resulting in integer frequency values. Although we chose moths of roughly the same age (approximately 2 days old), size (mean body length=53.21±2.34 mm) and mass (2.11±0.33 g), there may be many inter-individual differences between their flight ability, motivation or other physiological differences. Hence the data from all moths were not pooled but each moth was treated separately. For each moth however, the data from different flight bouts were pooled because the above differences were minimal from bout to bout.

A model for calculating the induced flow resulting from flapping wings appears in the companion paper (Sane, 2006). Here we test some specific predictions of that model. From the model, the equation for axial induced flow is given by:

$$v_{\text{axial}} = \left(\frac{\overline{C}_{\text{L}} \Phi n \bar{c} B_{\text{i}}}{\pi} \right) s_{\text{i}}(0) \,, \qquad (1)$$

where $\overline{C}_{\text{L}}$ is the average lift coefficient, Φ is the stroke amplitude, n is the wing beat frequency $\bar{c}$ is the mean chord length and $s_{\text{i}}(0)$ is a wing-shape dependent parameter (Sane, 2006). Because it is derived from propeller theory, this equation assumes a constant angle of attack during the stroke and predicts that, for a given wing shape and stroke amplitude, the induced axial velocity is directly proportional to the wing beat frequency.

As seen in Fig. 5, there is a large variability in the measured airspeed at any value of wing beat frequency. Similarly, at any given mean induced airspeed, there may be some variability in the wing beat frequency because other kinematic variables such as angle of attack, stroke amplitude or stroke position also influence induced airflow (Sane and Dickinson, 2001). Even

with these caveats, the two regressions show significant r^2 values (Table 2) suggesting that the model prediction (Sane, 2006) of a linear relationship between induced airflow and wing beat frequency is valid in the limited range of variability in wing beat frequency. Furthermore, the range of measured values of mean induced flow velocity lies within the range prescribed by the model (Fig. 5, grey region) in the corresponding frequency range.

It is important to note that Eqn 1 assumes that the fluid is inviscid and irrotational. This assumption holds for higher Reynolds number flows occurring at higher wing beat frequency, but may not accurately represent flows at Reynolds numbers below about 100 corresponding to very low wing beat frequency. Hence, Eqn 1 may not be extrapolated to zero wing beat frequency and the linear relationship between axial velocity and wing beat frequency predicted by this equation holds only in a high frequency range. Thus although we provide the values of y-intercept for completeness, these values do not provide any information about the relationship between wing beat frequency and mean airflow at very low values of wing beat frequency.

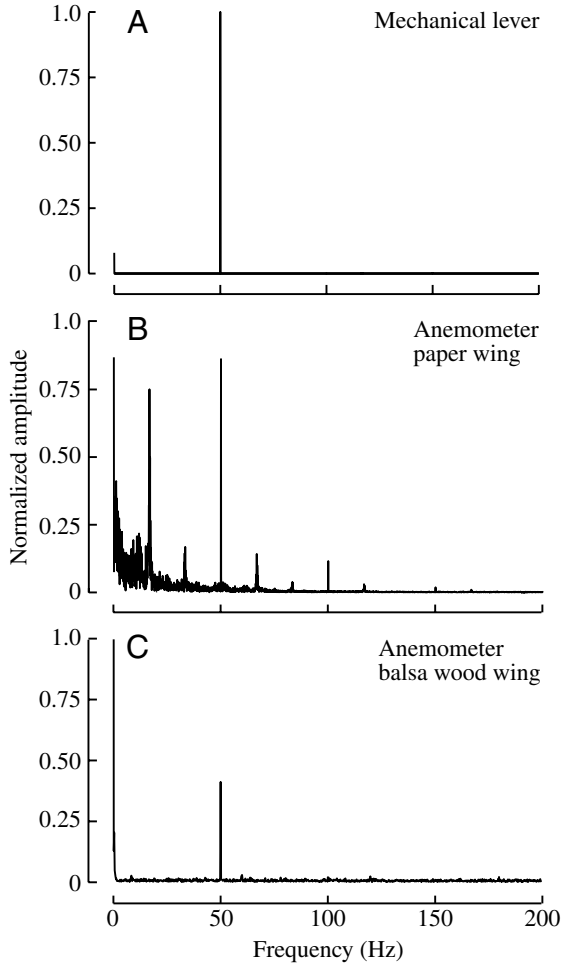

Fig. 6. Driven oscillations of artificial flexible and rigid wings. A mechanical lever attached to a servomotor and driven at 50 Hz (A) oscillated a flexible paper plate and a rigid plate made of balsa wood of the same dimensions and weight. Recordings from an anemometer placed near the paper plate (B) and balsa wood plate (C) show that the flexible plate has several frequency peaks for the driving frequency of 50 Hz, whereas the balsa wood plate has only a single peak at exactly 50 Hz.

Aerodynamic signature of wing flutter

One hypothesis of the higher frequency peaks is that they result from flutter phenomena in the wings. Alternatively, these peaks could primarily arise from measurement artefacts due to limitations of the instrument e.g. rectification of signal due to its inability to sense the direction of airflow etc. To test these hypotheses, we compared the anemometric records of the flexible paper wing with that of the rigid balsa wood wing when both were oscillated at 50 Hz. Like natural wings, the paper wings are flexible and flutter during rapid oscillations thus generating air disturbances that occur not only at the driving frequency but also at higher frequencies. In contrast, balsa wood offers a rigid non-aeroelastic alternative to reduce the flutter. If the double frequency peak is a measurement artefact, then it should be present in the frequency signature of both the flapping of rigid and flexible wings. At this frequency, however, the double frequency peak is absent from the frequency signatures of rigid wings (Fig. 6B), whereas it is present in the frequency signatures of flexible wings (Fig. 6C). The paper wing also shows contributions at twice and thrice the flapping frequency in addition to some lower frequency peaks, whereas the rigid wing shows a single peak at the flapping frequency. Because the motion of the servomotor lever was exactly the same in both cases and because the dimensions of the plates are also the same, these results suggest that the higher frequency peaks in the anemometric record arise from fluttering in a flexible wing rather than measurement artefacts. Thus, the higher frequency effects we measure are likely to be the aerodynamic consequence of the higher frequency components of the airfoil motion in flexible wings. These results agree well with the Fourier transform of the actual movement of the flexible wings (Combes and Daniel, 2003; see Fig. 7B). Together these results show that hot wire anemometry can be a useful tool for quantifying and analyzing the aerodynamic signature of fluttering wings. This phenomenon will be investigated in greater detail in a future research.

Discussion

Measurements of flow on flapping wings

This study highlights the complexity of flows around the body of a flying insect. As noted before, a number of biological processes are profoundly influenced by the dynamics of flow on the body of an insect. The measurements of induced airflow in this paper, in particular, allowed us to test specific predictions of the model for calculating induced flow proposed in a companion paper. Specifically, the mean induced airflow measured in the experiments reported here falls well within the range predicted by Eqn 1. With the knowledge of shape

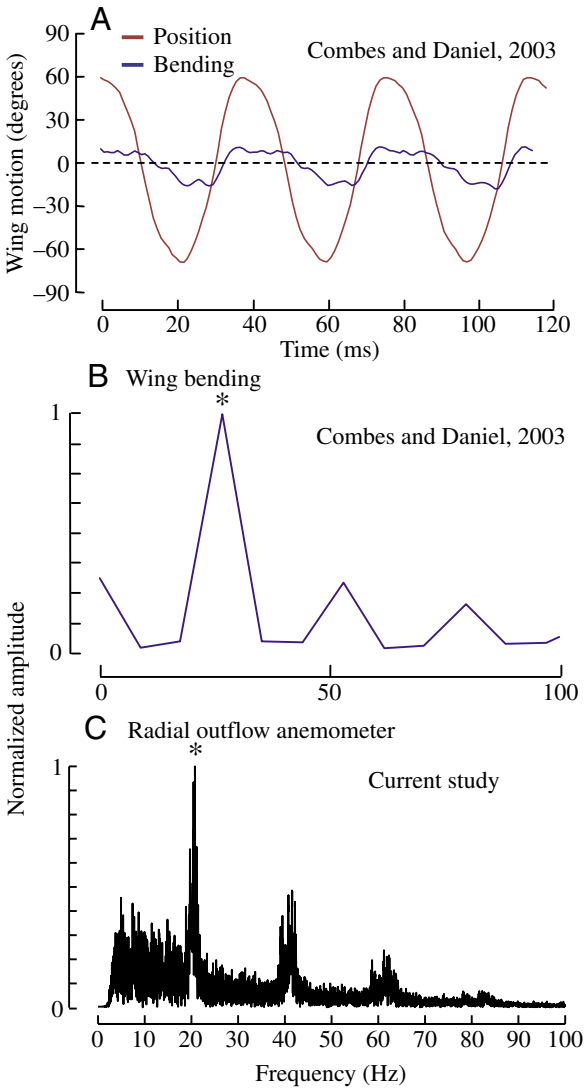

Fig. 7. Aerodynamic signature of wing flutter using anemometry. (A,B) Values replotted from the data of Combes and Daniel (2003) show the wing movements in terms of wing position and wing bending (excursion of trailing edge) as a function of time (A). These data were taken for a wing oscillated at frequencies typical of *Manduca sexta*. A Fourier analysis of the wing bending reveals frequency peaks at wing beat frequency and twice the wing beat frequency (B) similar to the frequency peaks measured in the trailing edge anemometric record (C).

parameters and wing kinematics, it is also possible to use Eqn 1 to estimate average lift coefficient in hovering flight of various insects through measurements of the axial inflow velocities. Although anemometric or the more detailed particle image velocimetry measurements of axial inflow in freely flying animals are usually difficult, they are becoming increasingly accessible in some insects (flies, Dickinson and Gotz, 1996; moths, Bomphrey et al., 2005) and hummingbirds (Warrick et al., 2005). These studies allow us to test the predictions of the model for gross near-field and far-field flow velocities. The model does not however predict higher order effects such as those occurring at wing beat frequency or higher. In contrast, the fine temporal resolution of hot wire anemometry, while spatially limited, affords new insights into the aerodynamics of flying insects. Hot wire anemometry has been used in only a few previous studies on animal flight (Bennett, 1970; Norberg et al., 1993; Lehmann, 1994) however these measurements were not concerned with the spectral characteristics over a broad frequency range. Here we show the first order effects such as mean induced flow from anemometric data, in addition to disturbances occurring at wing beat frequency and events occurring multiple times during each wing beat.

Effect of wing flutter on induced airflow

The high sensitivity of the anemometric records and the high sampling rate used in these experiments allow us to be reasonably certain that the higher frequency peaks (Fig. 4, Table 1) observed in the anemometric records arise from aerodynamic disturbances occurring at these frequencies. Because anemometers are mechanically decoupled from the rest of the apparatus, these peaks are unlikely to be measurement artefacts.

To test the hypothesis that the higher peaks arise from wing flutter, we measured the aerodynamic signature of artificial rigid *vs* flexible wings using hot wire anemometers. In oscillating flexible wings, we would expect flutter to cause aerodynamic disturbances primarily at the driving frequency but also at smaller or larger frequencies depending stiffness values of the material bending properties. Hence, in carefully controlled situations, any multiple frequency peaks observed in these anemometric measurements must arise from wing flutter. Conversely, because flutter is absent in a rigid wing, the multiple frequency peaks must be absent from anemometric measurements on rigid wings. The results shown in Fig. 6 suggest that the higher frequency peaks arise principally from wing flutter phenomena. Flexible paper wings oscillated by a mechanical lever at 50 Hz show peaks not only at 100 Hz. but also at 12.5, 25 and 75 Hz. In contrast, a rigid balsa wood wing, with the same mass and similar dimensions as the paper wing, shows a prominent peak only at the driving frequency of 50 Hz. Because all other experimental conditions were carefully controlled and the only variable was wing flexibility, the higher and lower frequency peaks in the aerodynamic signature can only be interpreted as resulting from wing flutter.

If true, these results predict that the actual motion of the flexible wings must also show similar higher frequency peaks. Fig. 7B shows the Fourier transforms of actual wing motion from Combes and Daniel (2003) compared to the Fourier transform aerodynamic signature of one of the moths in this study (Fig. 7C). Both records clearly show frequency peaks at two and three times the wing beat frequency. Together, these results strongly argue that the multiple frequency terms in the induced airflow records are influenced by wing flutter. We cannot, however, rule out contributions due to other phenomena such as the rapid efflux–influx of air due to the

near clap-and-fling events at the end of every upstroke (Ellington et al., 1996; Lehmann et al., 2005) or to the aerodynamic effects of wing rotation at either each stroke reversal (Dickinson et al., 1999; Sane and Dickinson, 2002). If the contributions of these phenomena are minimal, then hot wire anemometry in the near field offers us a simple method to quantify the aerodynamics of flutter in the wings of larger insects and birds.

The biological relevance of induced airflow

The effect of phasic airflow on airflow sensing in insects

Induced flow is a necessary byproduct of high Reynolds numbers fin-based or wing-based locomotion such as swimming or flying. As illustrated by this case study of *Manduca sexta*, there is both a phasic and a tonic component in the induced airflow around the mechanosensory structures. The phasic signal has a primary contribution from wing beat frequency and smaller tonic components at higher multiples of wing beat frequency arise from wing flexibility, and perhaps other phenomena such as clap-and-fling or wing rotation. The experiments reported here were performed on tethered moths flapping in absence of visual stimuli. However, visual stimuli play an important role in the control of wing kinematics in *Manduca sexta* (Frye, 2001) and are thus likely to add further complexity to the overall magnitude of induced air flow. Thus, the actual air speed experienced by the sensory structures of flying insects may be highly complex and dependent on their sensory environment.

The periodic fluctuations in air flow due to stroke frequency provide the timing cues that insects may use to tune their wing motion. The evidence for this hypothesis comes primarily from extensive work on locust flight. In a series of experiments, Horsmann et al. (1983) showed that tethered locusts flying in a wind tunnel coordinate the phase of their flight muscle activity in response to the phase of an external air flow varied within 3 Hz of the wing beat frequency of the locusts. This coordination was achieved primarily *via* mechano-sensory head hairs stimulated by the external airflow. There is also strong evidence that locusts coordinate their wing movements with the periodic disturbances to the external airflow, such as the presence of another locust beating its wings upstream (Kutsch et al., 1994). Together, these studies suggest that induced airflow provides an important timing signal, allowing the mechanosensory organs of flying animals to finely tune their wing kinematics and synchronize their wing movements with the neighboring insects during aggregation or swarming.

Effect of mean and phasic airflow on odor tracking in moths

Previous work on the flightless moth *Bombyx mori* has elucidated how flapping wings can significantly enhance the flux of air over the antenna, thereby increasing the effective volume of air sampled for odors (Loudon and Koehl, 2000). Because active flight typically demands higher wing amplitudes and wing beat frequencies than the flightless case, enhancement of odor sampling is likely to be even more pronounced during active flight.

Yet, in spite of its potential importance, the possibility that flying enables a better sampling of odor has received very little attention in most studies on odor tracking. The influence of wings on olfactory processes may be quite significant. The experiments reported here show that in hovering or stationary moths, there is significant upwind disturbance to the odor plumes and very likely an alteration of the filamentous structure of the incoming plumes. In hovering moths, practically all of the airflow experienced at the antennae results from entrained induced flow. With increasing ambient flow, the upwind disturbance due to flapping wings decreases. Thus, under windless conditions the pheromone or odor plumes may not retain much directional information after they are entrained by the wings, thus interfering with the insect's ability to precisely determine the source direction by purely olfactory means.

Accounting for self-generated airflow is also likely to provide new insights into the timescales involved in odor discrimination. Because the fine structure of odor plumes influences the orientation of flying moths (Mafra-Neto and Carde, 1994), it is important to determine the alterations to plume structure in the vicinity of the antennae of a flying moth and its effect on odor tracking. For example, a series of recent experiments on the moth *Helicoverpa zea* suggest that these moths are able to distinguish between pheromone and antagonist odor sources separated by at most 1 ms or 1 mm distance when tracking odor plumes in a wind tunnel (Baker et al., 1998; Fadamiro et al., 1999). In these moths, individual sensilla may contain at least two receptors, one sensitive to pheromone and another to antagonistic odor. The co-compartmentalization of these two neurons allows them to sample odors at a single point in space and time and thus report on the synchronous arrival of the two odors in a well-blended plume, thereby suppressing upwind flight to an interspecific odor source. However, even the slightest separation (estimated at 1 ms in time or 1 mm in distance) between the pheromone and antagonist filaments detected by these moths indicates the presence of a conspecific female in presence of other interspecific females and thus elicits plume tracking behavior. Our studies suggest that if we take induced velocity into account, the relative velocity of the plume strands with respect to the moth antenna may be even greater than estimated previously, and thus the estimate of temporal separation between the two odor plumes is likely to be well under the 1 ms value reported in literature. Likewise, the spatial separation is also likely to be lower than previously estimated. Further, an upwind mixing of these plumes during flight is likely to blend the odor plumes to a greater degree before they reach the moth's antenna.

It is also well known that moths show a better response to pulsatile odor delivery as compared to uniformly distributed odors (Baker et al., 1985). Our results also suggest that an inherent pulsatility to odor delivery, arising with each wing flap, exists in all flapping moths regardless of the ambient plume structure and will further amplify this effect. Thus, the mere initiation of flapping is likely to enhance the response to

odor while compromising the resolution between individual filaments of odor plumes.

Effect of mean induced airflow on thermoregulation in insects

In many insects, flight is possible only after the thoracic temperature rises above a certain threshold value, well above the ambient temperature. In *Manduca sexta* and other moths, this value is attained by muscle thermogenesis through rapid wing vibration (shivering), whereas in some other insects it is attained by behavioral themoregulatory mechanisms such as basking in the sun. Forced convection is the main agent of heat loss as compared to evaporative or radiative heat loss in insects (Church, 1959). In hovering insects, the heat loss due to induced airflow is particularly important. For instance in *Manduca sexta*, samples of the speed of this airflow (shown in Fig. 3) measured by the axial inflow anemometer ranged from 0 to 0.52 m s^{-1} whereas the radial outflow anemometer, which measures flow enveloping the insect's body, measured a typical range between 0.25 to 3.55 m s^{-1} during flight. Although these flows are of comparable magnitude to the airflow relative to body arising from the moth's motion in air (observed mean horizontal speed of 3.6 m s^{-1}; Stevenson et al., 1995), there are very few published estimates on forced convection in flying insects account for induced airflow (but see May and Casey, 1983; Borrell and Medeiros, 2004). The induced flow at the outflow location for the bumblebee *Bombus terrestrus* is estimated at approximately 1.8 m s^{-1} (Dudley and Ellington, 1990a,b), also significant compared to their maximum forward flight speeds of 5–6 m s^{-1} (Ellington, 1999). Similarly, in *Drosophila melanogaster* (not a thermoregulating insect), induced flow at the antennae is estimated at 0.15 m s^{-1} and higher by a factor of 2–5 at the outflow location, and are a significant percentage of their typical top flight speeds of 0.45–0.8 m s^{-1} (Marden et al., 1997; Frye et al., 2003). Indeed, the flow immediately behind the wings is likely always to be significant compared to forward flight speeds in most insects.

In the case of *Manduca sexta*, cooling rates vary rapidly as the air flow speed increases rapidly from 0 to 3 m s^{-1} before slowly attaining a plateau at values higher than 5 m s^{-1} (Heinrich, 1971). When calculating convective heat losses, the value of air flow used in the calculation is usually the relative velocity of the moth in air, i.e. with respect to far-field flow. For the case of hovering moths, these calculations would therefore predict very little heat loss due to convection. Our studies show that when we account for self-generated airflow, the calculated heat loss would be substantially higher. A mean self-generated airflow of approximately 1.5 m s^{-1}, typical of hovering hawk moths, doubles the estimated cooling rates.

As shown in Fig. 5 and Table 2, the induced airflow increases with wing beat frequency, thereby further enhancing the cooling of the body. However, because an increase in wing beat frequency is also associated with greater heat generation within the thorax due to greater muscle activity, it is unlikely that insects increase their wing beat frequency to actively cool down during flight. However it is likely to be less effective at increasing thoracic temperatures than has been previously thought and induced airflow must be taken into account when considering the hypothesis that insects actively increase wing beat frequency for thermoregulation.

Similarly, just as the pulsatile mean fields due to induced flow augments transport of odors and heat, they would also augment a host of other flow-mediated transport processes including gas exchange and water loss, and hence it is important for researchers studying these phenomena in flying insects to account for the influence of induced flow due to flapping wings.

We are deeply grateful to Tom Daniel, Michael Dickinson and Ty Hedrick for their comments and to Mark Willis and Michael Dillon for numerous discussions. This work was supported by an NSF Inter-Disciplinary Informatics grant to Sanjay Sane and an Office of Naval Research MURI to Tom Daniel and C. Diorio.

References

Baker, T. C., Willis, M. A., Haynes, K. F. and Phelan, P. L. (1985). A pulsed cloud of sex-pheromone elicits upwind flight in male moths. *Physiol. Entomol.* **10**, 257-265.

Baker, T. C., Fadamiro, H. Y. and Cosse, A. A. (1998). Moth uses fine tuning for odour resolution. *Nature* **393**, 530.

Bennett, L. (1970). Insect flight: lift and the rate of change of incidence. *Science* **167**, 177-179.

Bomphrey, R. J., Lawson, N. J., Harding, N. J., Taylor, G. K. and Thomas, A. L. R. (2005). The aerodynamics of *Manduca sexta*: digital particle image velocimetry analysis of the leading-edge vortex. *J. Exp. Biol.* **208**, 1079-1094.

Borrell, B. J. and Medeiros, M. J. (2004). Thermal stability and muscle efficiency in hovering orchid bees (Apidae: Euglossini). *J. Exp. Biol.* **207**, 2925-2933.

Brodsky, A. K. (1991). Vortex formation in the tethered flight of the peacock butterfly *Inachis io* L. (Lepidoptera, Nymphalidae) and some aspects of insect flight evolution. *J. Exp. Biol.* **161**, 77-95.

Church, N. S. (1959). Heat loss and the body temperatures of flying insects. II. Heat conduction within the body and its loss by radiation and convection. *J. Exp. Biol.* **37**, 186-212.

Combes, S. A. and Daniel, T. L. (2003). Into thin air: contributions of aerodynamic and inertial-elastic forces to wing bending in the hawkmoth *Manduca sexta*. *J. Exp. Biol.* **206**, 2999-3006.

Dickinson, M. H. and Gotz, K. G. (1996). The wake dynamics and flight forces of the fruit fly *Drosophila melanogaster*. *J. Exp. Biol.* **199**, 2085-2104.

Dickinson, M. H., Lehmann, F. O. and Sane, S. P. (1999). Wing rotation and the aerodynamic basis of insect flight. *Science* **284**, 1954-1960.

Dudley, R. and Ellington, C. P. (1990a). Mechanics of forward flight in bumblebees. I. Kinematics and morphology. *J. Exp. Biol.* **148**, 19-52.

Dudley, R. and Ellington, C. P. (1990b). Mechanics of forward flight in bumblebees. II. Quasi-steady lift and power requirements. *J. Exp. Biol.* **148**, 53-88.

Ellington, C. P. (1999). The novel aerodynamics of insect flight: Applications to micro-air vehicles. *J. Exp. Biol.* **202**, 3439-3448.

Ellington, C. P., vandenBerg, C., Willmott, A. P. and Thomas, A. L. R. (1996). Leading-edge vortices in insect flight. *Nature* **384**, 626-630.

Fadamiro, H. Y., Cosse, A. A. and Baker, T. C. (1999). Fine-scale resolution of closely spaced pheromone and antagonist filaments by flying male *Helicoverpa zea*. *J. Comp. Physiol. A* **185**, 131-141.

Frye, M. A. (2001). Effects of stretch receptor ablation on the optomotor control of lift in the hawkmoth *Manduca sexta*. *J. Exp. Biol.* **204**, 3683-3691.

Frye, M. A., Tarsitano, M. and Dickinson, M. H. (2003). Odor localization requires visual feedback during free flight in *Drosophila melanogaster*. *J. Exp. Biol.* **206**, 843-855.

Gewecke, M. (1970). Antennae – Another wind-sensitive receptor in locusts. *Nature* **225**, 1263.

Grodnitsky, D. L. and Morozov, P. P. (1992). Flow visualization experiments on tethered flying green lacewings *Chrysopa dasyptera*. *J. Exp. Biol.* **169**, 143-163.

Heinrich, B. (1971). Temperature regulation of sphinx moth, *Manduca sexta*: I. Flight energetics and body temperature during free and tethered flight. *J. Exp. Biol.* **54**, 141-152.

Heinrich, B. (1993). *The Hot-Blooded Insects*. Cambridge: Harvard University Press.

Horsmann, U., Heinzel, H. G. and Wendler, G. (1983). The phasic influence of self-generated air current modulations on the locust flight motor. *J. Comp. Physiol.* **150**, 427-438.

Kutsch, W., Camhi, J. and Sumbre, G. (1994). Close encounters among flying locusts produce wing-beat coupling. *J. Comp. Physiol. A* **174**, 643-649.

Lehmann, F.-O. (1994). *Aerodynamische, Kinematische und Electrophysiologische Aspekte der Flugkrafterzeugung und Flugkraftsteuerung bei der Taufliege Drosophila Melanogaster*. Tübingen: Eberhad-Karls-Universität.

Lehmann, F. O., Sane, S. P. and Dickinson, M. (2005). The aerodynamic effects of wing-wing interaction in flapping insect wings. *J. Exp. Biol.* **208**, 3075-3092.

Loudon, C. and Koehl, M. A. R. (2000). Sniffing by a silkworm moth: Wing fanning enhances air penetration through and pheromone interception by antennae. *J. Exp. Biol.* **203**, 2977-2990.

Mafra-Neto, A. and Cardé, R. T. (1994). Fine-scale structure of phenomone plumes modulates upwind orientation of flying moths. *Nature* **369**, 142-144.

Marden, J. H., Wolf, M. R. and Weber, K. E. (1997). Aerial performance of *Drosophila melanogaster* from populations selected for upwind flight ability. *J. Exp. Biol.* **200**, 2747-2755.

May, M. L. and Casey, T. M. (1983). Thermoregulation and heat-exchange in Euglossine bees. *Physiol. Zool.* **56**, 541-551.

Norberg, U. M., Kunz, T. H., Steffensen, J. F., Winter, Y. and Vonhelversen, O. (1993). The cost of hovering and forward flight in a nectar-feeding bat, *Glossophaga soricina*, estimated from aerodynamic theory. *J. Exp. Biol.* **182**, 207-227.

Percival, D. B. and Walden, A. T. (1993). *Spectral Analysis for Physical Applications. Multi-taper and Conventional Univariate Techniques*, p. 583. Cambridge: Cambridge University Press.

Roberts, S. P. and Harrison, J. F. (1998). Mechanisms of thermoregulation in flying bees. *Am. Zool.* **38**, 492-502.

Sane, S. P. (2003). The aerodynamics of insect flight. *J. Exp. Biol.* **206**, 4191-4208.

Sane, S. P. (2006). Induced airflow in flying insects. I. A theoretical model of the induced flow. *J. Exp. Biol.* **209**, 32-42.

Sane, S. P. and Dickinson, M. H. (2001). The control of flight force by a flapping wing: lift and drag production. *J. Exp. Biol.* **204**, 2607-2626.

Sane, S. P. and Dickinson, M. H. (2002). The aerodynamic effects of wing rotation and a revised quasi-steady model of flapping flight. *J. Exp. Biol.* **205**, 1087-1096.

Srygley, R. B. and Thomas, A. L. R. (2002). Unconventional lift-generating mechanisms in free-flying butterflies. *Nature* **420**, 660-664.

Stevenson, R. D., Corbo, K., Baca, L. B. and Le, Q. D. (1995). Cage size and flight speed of the tobacco hawkmoth *Manduca sexta*. *J. Exp. Biol.* **198**, 1665-1672.

Vickers, N. J. (2000). Mechanisms of animal navigation in odor plumes. *Biol. Bull.* **198**, 203-212.

Warrick, D. R., Tobalske, B. W. and Powers, D. R. (2005). Aerodynamics of hovering hummingbird. *Nature* **435**, 1094-1096.

Wasserthal, L. T. (2001). Flight-motor-driven respiratory air flow in the hawkmoth *Manduca sexta*. *J. Exp. Biol.* **204**, 2209-2220.

Willis, M. A. and Arbas, E. A. (1991). Odor-modulated upwind flight of the sphinx moth, *Manduca sexta* L. *J. Comp. Physiol. A* **169**, 427-440.

Willis, M. A. and Baker, T. C. (1984). Effects of intermittent and continuous pheromone stimulation on the flight behavior of the oriental fruit moth, *Grapholita molesta*. *Physiol. Entomol.* **9**, 341-358.

Willmott, A. P., Ellington, C. P. and Thomas, A. L. R. (1997). Flow visualization and unsteady aerodynamics in the flight of the hawkmoth, *Manduca sexta*. *Phil. Trans. R. Soc. Lond. B* **352**, 303-316.